Autonomous OA Removal in Real-Time from Single Channel EEG Data on a Wearable Device Using a Hybrid Algebraic-Wavelet Algorithm

CHARVI A. MAJMUDAR and BASHIR I. MORSHED, University of Memphis

Electroencephalography (EEG) is a non-invasive technique to record brain activities in natural settings. Ocular Artifacts (OA) usually contaminates EEG signals, removal of which is critical for accurate feature extraction and classification. With the increasing adoption of wearable technologies, single-channel real-time EEG systems that often require real-time signal processing for immediate real-time feedback are becoming more prevalent. However, traditional OA removal algorithms usually require multiple channels of EEG data, are computationally expensive, and do not perform well in real-time. In this article, a new hybrid algorithm is proposed that autonomously detects OA and subsequently removes OA from a single-channel steaming EEG data in real-time. The proposed single EEG channel algorithm also does not require additional reference electrooculography (EOG) channel. The algorithm has also been implemented on an embedded hardware platform of single channel wearable EEG system (NeuroMonitor). The algorithm first detects the OA zones using an Algebraic approach and then removes these artifacts from the detected OA zones using the Discrete Wavelet Transform (DWT) decomposition method. The de-noising technique is applied only to the OA zone, which minimizes loss of neural information outside the OA zone. A qualitative and quantitative performance evaluation was carried out with a 0.5s epoch in overlapping sliding window technique using time-frequency analysis, mean square coherence, and correlation coefficient statistics. The hybrid OA removal algorithm demonstrated real-time operation with 3s latency on the PSoC-3-microcontroller-based EEG system. Successful implementation of OA removal from single-channel real-time EEG data using the proposed algorithm shows promise for real-time feedback applications of wearable EEG devices.

CCS Concepts: • **Computer systems organization** → **Embedded systems**; Real-time system architecture

Additional Key Words and Phrases: Artifact removal, EEG signal processing, real-time algorithm, wearable

ACM Reference Format:
Charvi A. Majmudar and Bashir I. Morshed. 2016. Autonomous OA removal in real-time from single channel EEG data on a wearable device using a hybrid algebraic-wavelet algorithm. ACM Trans. Embed. Comput. Syst. 16, 1, Article 20 (October 2016), 16 pages.
DOI: http://dx.doi.org/10.1145/2983629

1. INTRODUCTION

Electroencephalography (EEG) is the depiction of the neurological signals in terms of the electrical signals corresponding to the brain activities non-invasively from the scalp's surface using EEG electrodes (typically Ag/AgCl) interfaced with a conductive media [Peng et al. 2011]. The greatest advantages of EEG are its high temporal resolution, low equipment cost, and non-invasive procedure [Morshed and Khan 2014; Teplan 2002], EEG signals are widely used to study the brain's connectivity, plasticity, and organization of cognitive processes such as perception, memory, attention, language,

Authors' addresses: C. A. Majmudar and B. I. Morshed, Department of Electrical and Computer Engineering, The University of Memphis, Memphis, TN 38152; emails: {cmjmudar, bmorshed}@memphis.edu.

DOI: http://dx.doi.org/10.1145/2983629

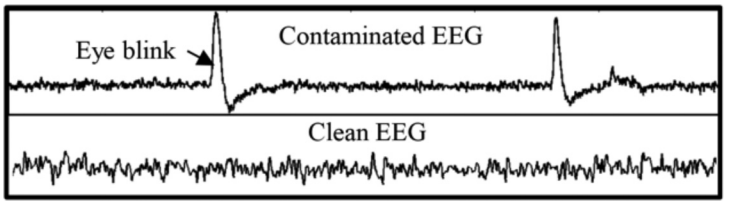

Fig. 1. A representative EEG signal with OA vs. an EEG signal without OA.

and emotion in normal adults and children [Chi et al. 2013]. The data produced by EEG systems are commonly used to investigate information about certain disorders such as epilepsy, Alzheimer's disease, ADHD (Attention-Deficit/Hyperactive Disorder) etc. for diagnosis and therapy efficacy. Real-time implementation of wearable monitoring and therapy systems for epilepsy, cognitive activities, and other medical applications are promising [Masse et al. 2013; Nam et al. 2013]. Electrical signals of EEG systems are detected along the scalp and include both neuronal signals originating from cerebral lobes as well as from non-cerebral origins, such as muscular activities, which are called *artifacts*. The physiological artifacts can be due to any minor body movements, EMG (Electromyography), ECG (pulse, pace-maker), eye movements, sweating, etc. These artifacts can occur in the same spectral bands of neuronal signals and can be very difficult to remove without the loss of critical neuronal information concurrent to the occurrence of the artifacts. However, most automated artifact removal methods do not capture neuronal information during the OA event, and may alter neuronal information outside the OA region [Cassani et al. 2014]. Figure 1 depicts an example of a typical raw EEG data (from FP1 location) with ocular artifacts (OA), and the neuronal signals without OA.

This work focuses on removal of physiological artifacts arising from eye-blinks and movement of the eyeballs, which are collectively known as Ocular Artifacts (OA) while preserving as much neuronal information as possible. Regular EEG signals in the order of microvolts are contaminated by these OA in the order of millivolts. The frequency range of interest for most of the EEG applications lies up to 100Hz, and typical amplitude is 0.5μV to 100μV [Teplan 2002] whereas OA occurs within the range of 0Hz to 16Hz having amplitude more than 10 times the regular cortical signals [Joyce et al. 2004]. In today's wearable technology, EEG devices are also becoming increasingly portable in nature and thus lighter in weight. Safety critical medical applications are also emerging, such as monitoring infants within the limited space of a humidified incubator [Lloyd et al. 2015]. Often, Alzheimer's and epilepsy disease recognition are also based on EEG systems [Tiganj et al. 2010]. To accomplish this critical and medically relevant applications of the EEG recordings, in addition to health-and-wellness-related applications, single-channel EEG devices are expected to become more relevant and convenient. This motivated us to develop an OA removal algorithm that is: (a) applicable to single-channel EEG devices, (b) executable in real-time, and (c) implementable on microcontroller-based embedded hardware. Based on these requirements, the detailed literature review was carried out for the methods applicable only to the single-channel EEG having minimum processing time with low complexity. Some related methods reported in the literature are Wavelet Transform (WT) [Ramanan et al. 2004; Krishnaveni et al. 2006; Kumar et al. 2008], EMD (Empirical Mode Decomposition), CCA (Canonical Correlation Analysis) [Soomro et al. 2013; Sweeney et al. 2013], Modified Multiscale Sample entropy (mMSE)-wICA [Mahajan and Morshed 2015], and Algebraic Method (AM) [Tiganj et al. 2010]. WT is considered to be promising for its ability to OA removal on a single-channel EEG [Ramanan et al. 2004; Krishnaveni

Table I. Formulae Utilized for OA Detection Using AM

Impulse response equation	$h_k(t_m) = \frac{(-1)^{k+1}}{(v-1)!}\frac{d^2}{dt_m^2}(1+t_m)^{k+2}t_m^{v-1}; 0 \leq t_m \leq T$ $= 0$; elsewhere	
Coefficients calculation using FIR Filter	$v_k(\tau) \approx v_{k,n} = \sum_{m=0}^{M} W_m h_{k,m} y_{n+M-m}$	
Decision function calculation	1.	$F_{k,n} = \left[v_{k+1,n}\right]^2 - v_{k,n}v_{k+2,n}$
	2.	$F_n = \prod_{k=0}^{K-1} F_{k,n}$; $n = 0, 1, 2 \ldots$
Threshold equation	$\gamma = N / (\mu + \sigma)$; N = Constant; μ = mean; σ = Standard Deviation	

et al. 2006; Kumar et al. 2008]. The methods described in Soomro et al. [2013] and Sweeney et al. [2013] were similar to the WT method in terms of signal processing and performance, but the computational cost was higher than the WT algorithm. The mMSE-based algorithm [Mahajan and Morshed 2015] required more than one EEG channel, whereas the AM detects only the OA zone [Tiganj et al. 2010]. It was shown by Tiganj et al. [2010] that AM is very fast in terms of processing time as compared to the WT-based algorithm for OA detection. OA removal from online EEG data has also been demonstrated, but these algorithms require access to multiple channels of EEG data [Mahajan 2015; Noureddin 2010], which has degraded performance if the number of channels is few, and not suitable for single-channel EEG systems. Following up our previous work [Majmudar et al. 2015], where the hybrid OA removal algorithm was implemented for single-channel EEG using MATLAB software, this article extends the work by implementing the proposed hybrid algorithm on our custom NeuroMonitor (NM) EEG system with microcontroller (MCU) hardware [Consul-Pacareu et al. 2014]. The proposed fully autonomous algorithm first detects the OA using AM and then removes artifacts only from the detected OA zones using Discrete WT (DWT) based method. The MCU implemented this hybrid OA removal algorithm and executed in real-time for single-channel EEG as described in this article.

2. METHODOLOGY

In this section, we discuss the methods used for identifying and de-noising the ocular zones in the raw EEG data in real time.

2.1. Algebraic Approach for OA Zone Detection

Algebraic Method (AM) detects abrupt changes in signal and estimates their locations for the noisy observations $y(t)$ of a piece-wise regular signal $x(t)$ [Mboup 2012]. AM to detect OA zone has a fast processing time, a suitable feature for real-time applications [Majmudar et al. 2015]. AM considers that there exists at most one spike in each interval $I\,[\tau, \tau + T]$, where, τ is the origin and T is the length of I. In this interval, Finite Impulse Response (FIR) filter of the order M is applied to extract FIR filter coefficients using the sliding window technique, which is repeated n times, where n represents the number of sliding windows in interval T. Next, using the cumulative effect of the FIR filter coefficients for all windows, the Decision function, Fn, is calculated, and iff that value exceeds the threshold, a spike exists at time tk. Table I shows the required mathematical formulae to implement the algebraic algorithm [Tiganj et al. 2010].

For OA zone detection using AM, $y(t)$ is the raw EEG signal (sampled at 256sps) and $x(t)$ is a small epoch of 0.5s to be processed in real-time for a single channel EEG. The epoch length is chosen to match the typical OA durations so that there can only

Table II. DWT (Haar) Formulae for OA Removal

DWT (Haar)	$a_n = \frac{f_{2m-1} + f_{2m}}{\sqrt{2}}; d_n = \frac{f_{2m-1} - f_{2m}}{\sqrt{2}}$
Inverse DWT	$f = \left(\frac{a_1 + d_1}{\sqrt{2}}, \frac{a_1 - d_1}{\sqrt{2}}, .., \frac{a_{N/2} + d_{N/2}}{\sqrt{2}}, \frac{a_{N/2} - d_{N/2}}{\sqrt{2}}\right)$
	a_n = Approximate Coefficient ; d_n = Detail Coefficient

be a single OA in an epoch. The threshold equation parameter (referenced from Krishnaveni et al. [2006]) N is fixed to 0.0001 based on trial-and-error to trigger detection of only the OA in the given epoch and not trigger for only neuronal signals. This algorithm is implemented on a PSoC-3 microcontroller (Cypress Semiconductor Corp., San Jose, CA)-based NM EEG hardware platform. For the real-time processing to have low latency, the FIR filter order M has been taken as 38 for 0.15s epochs, half of the FIR filter order of 76 used in our previous offline algorithm work [Majmudar et al. 2015], as computation time is much faster with FIR order of 38 but still produces acceptable performance. For FIR filter realization on MCU, convolution algorithm steps were implemented. The OA detection algorithm described in this article was first implemented and verified using Visual Studio 2010 (Microsoft Corp., WA), and then was implemented using C language on PSoC-3 microcontroller hardware of NM device using the PSOC creator 3 Integrated Development Environment (IDE).

2.2. Discrete Wavelet Transform Based OA De-Noising

Wavelet Transform (WT) has emerged as one of the robust methods for processing non-stationary signals such as EEG. In this method, the input signal is convolved with high-pass and low-pass filters to get the detail and approximation coefficients, respectively, whose impulse response is determined by the wavelet chosen [Gorji et al. 2013].

Both the coefficients are then down-sampled by the factor of 2 before the next decomposition level. Also, at the end of every decomposition level, the input signal frequency band gets halved. Here, for the MCU implementation of DWT, the mother wavelet chosen is a Haar wavelet as it is the most hardware efficient for the real-time hardware implementation [Krishnaveni et al. 2006]. The Haar transform approximation coefficients are the running average (trends) whereas the detailed coefficients are the running difference (fluctuations). The required Haar wavelet DWT algorithm formulae implemented on PSOC-3 MCU for this method are mentioned in Table II.

In this work, DWT-based signal decomposition was performed using Haar wavelet for up to Level Seven based on the sampling rate (256sps) and the lowest frequency of interest for EEG bands (Delta at 0.5Hz). For the threshold-based de-noising, Levels 4 to 7 (between 0.5Hz to 16Hz) were compared with the threshold value. The same threshold value of the OA detection method (AM) was used. To preserve the low-frequency components in non-OA zones, DWT for OA removal is applied only to the detected OA zones (identified by AM as discussed above) to ensure that the critical EEG background information remains unaltered outside of OA region.

The proposed DWT-based OA removal algorithm steps are as follows:

2.3. Discrete Wavelet Transform-Based OA De-Noising

For the real-time single-channel raw EEG data streaming with minimum latency, intervals (*window*) of 128 samples (0.5s @ 256sps) are processed at a time in a block for reliable OA detection and OA removal. Larger interval sizes improve performance insignificantly but suffer from larger latency; while smaller interval sizes do not yield satisfactory performance. It must be noted that, for some blocks, the eye blinks might

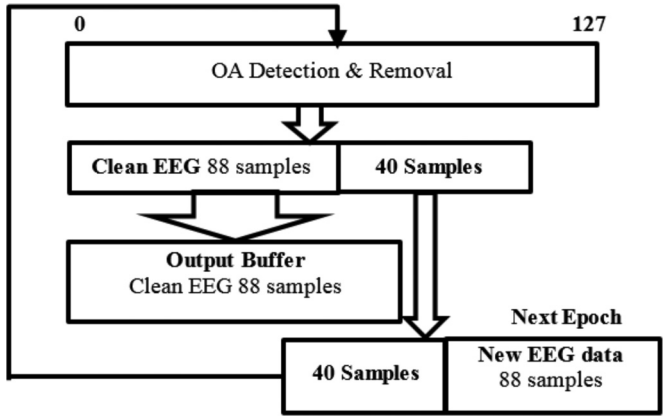

Fig. 2. Flow-chart of the EEG epoch overlapping technique.

ALGORITHM 1: OA Removal Algorithm

```
Input: Raw streaming EEG data.
repeat
  Using sliding window technique, obtain an epoch of data.
  Use Algebraic algorithm to detect if there is any OA within the epoch of data.
  if (OA detected)
    Apply DWT only to the detected OA zone
    Decompose it up to seven levels using Haar as a basis function.
    The detail coefficients of decomposition levels 4 to 7 are compared with the threshold.
    // This range corresponds to the frequency range of 0.5Hz to 16Hz.
    if (coefficient value > the threshold value)
      The coefficient is replaced with zero
    else
      The coefficient retains its value.
    end
    Perform inverse DWT to reconstruct the clean EEG signals from decomposed signals.
  end
until forever;
```

partially occur at the beginning or end of the epoch that might be undetected by the algorithm. To prevent these OA detection misses, we have implemented overlapping sliding windows by 31%, which ensures that the OA is detected at the previous or the next window. The robustness of this approach for correct OA zone detection was previously verified by testing it with several datasets in the offline analysis as previously reported [Majmudar et al. 2015]. The implemented EEG epoch overlapping technique for the hybrid OA removal algorithm is depicted in Figure 2. Out of the total epoch length of 128 samples, only the initial 88 samples were considered as the clean EEG after de-noising, whereas the last 40 samples were reconsidered for the next epoch processing to ensure correct OA detection, where OA lies at the edge of any epoch.

The entire overlapping method was implemented in real-time on NM PSOC-3 MCU using a ring buffer technique, as mentioned in Figure 3. The ring buffer had a length of 768 bytes. It uses *put-index* and *get-index* for storing analog to digital converter (ADC) sampled 16-bit raw EEG data (one channel) and for fetching the previously stored EEG sample for OA detection process, respectively. The race condition between *put-index* and *get-index* was monitored in main code before fetching a new block of 88 samples using *get-index* for OA detection.

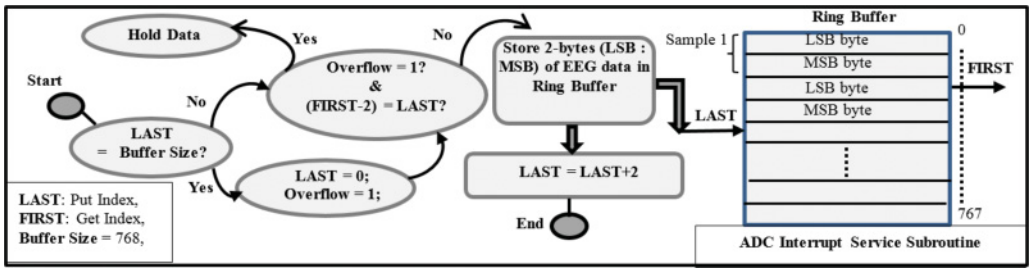

Fig. 3. Graphical presentation of ADC ISR execution steps for the PSOC-3 microcontroller.

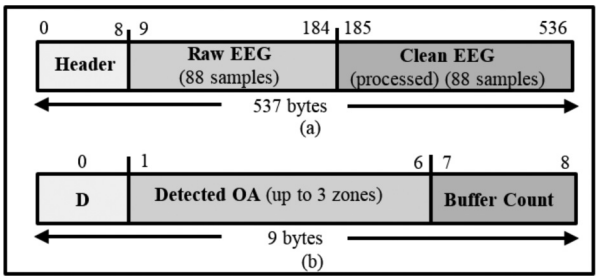

Fig. 4. (a) NM output packet formation, (b) 9-byte header formation.

For each epoch, the processed 88 samples at the output of the algorithm were transmitted wirelessly by the NM device via an output buffer. For the verification of the OA detection and OA removal algorithms, the output buffer of length of 537 bytes was formed in a predefined packet format prior to sending it wirelessly using Bluetooth (Figure 4). The output packet was comprised of three sections: Header section (9 bytes), raw EEG data from ADC (88 samples of 16-bit data = 176 bytes), and processed EEG data (88 samples of 32 bits float data = 352 bytes). Within the 9-bytes-long header, the 1st byte contained the packet type indicator designated as the ASCII character 'D' (for Data). This byte was extracted at the remote user console to authenticate the start of the received data packet. A sequential integer of 2 bytes for packet count was stored at the 8th and 9th position of the header. The 6 bytes from the 2nd to 7th positions can store up to three detected OA zone sample identifiers in a pairwise manner (starting edge and ending edge) per epoch.

2.4. Overall Hardware Implemented Hybrid Approach

The overall algorithm proposed in this article implements the algebraic approach (AM) to detect the OA zone and DWT-based de-noising technique applied only to the detected OA zones for OA removal (Figure 5). This algorithm was found to be suitable for real-time implementation for the single-channel EEG signal OA removal on a microcontroller-based hardware. The proposed method efficiently cleans OA while preserving neuronal information from detected OA zones using single channel DWT algorithm. Furthermore, the proposed method does not alter any neuronal information in the non-OA zones.

Some key considerations for implementing hybrid algorithm are mentioned below:

(a) The interval I in an Algebraic Method (AM) for OA detection has been taken as 0.15s (half of 0.29s [Majmudar et al. 2015]) to reduce the FIR filter order for the faster and efficient microcontroller-based algorithm execution.

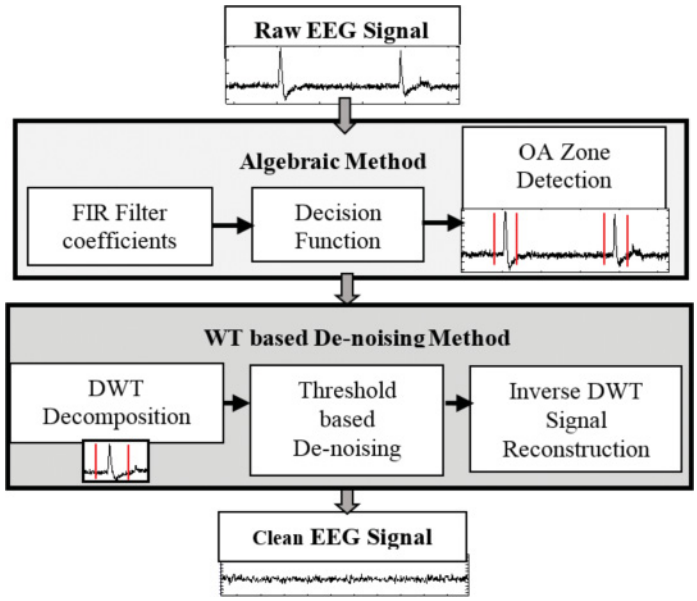

Fig. 5. Hardware-implemented overall EEG de-noising algorithm.

(b) The FIR filter delay, which is generally half of the filter order, was adjusted by calculating the OA zone locations [Majmudar et al. 2015].
(c) The ring buffer based on 128 samples of EEG epoch using the overlapping technique is implemented in real-time for single-channel EEG data to ensure OA detection at the edge of the epochs.

2.5. Performance Evaluation

For the validation and performance evaluation of the proposed OA removal technique, Time-Frequency Analysis (TFA), Magnitude Square Coherence (MSC) plot, and Correlation of Coefficient (CC) statistics were utilized. The TFA was carried out using EEGLAB [Delorme and Makeig 2004] built-in function. The TFA plot provides the information of spectral energy content variation with elapsed time. The MSC plot is generated using the MATLAB function '*mscohere*'. MSC gives the estimate of the frequency coherence between the two signals x and y, where values between 0 and 1 indicate how well signal x corresponds to signal y at each frequency. CC computes the similarity between the raw and corrected EEG signals. MATLAB (MathWorks Inc., Natwick, MA) function '*corrcoef*' is used to determine CC, which ranges between 0 and 1; 0 representing *no match at all* and 1 representing an *exact match*. CC is separately computed for the non-OA zone and the OA zone to clearly show the statistical correlation in respective zones.

3. TEST SETUP AND PROCEDURE

This section discusses the hardware and software utilized, data acquisition protocol, processing, and verification techniques used in the implementation of the algorithm. The block diagram depicting the overall implementation and remote evaluation procedure of the proposed hybrid algorithm is shown in Figure 6.

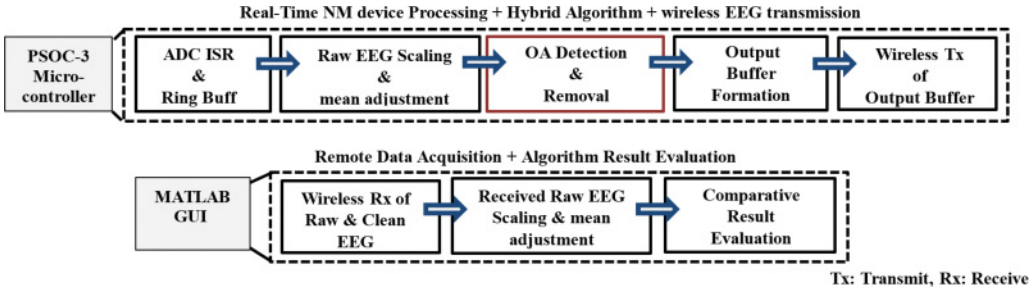

Fig. 6. Block diagram depicting the hardware implemented the real-time hybrid algorithm for OA removal at the wearable device with a PSOC-3 microcontroller and the real-time comparison at the remote computer.

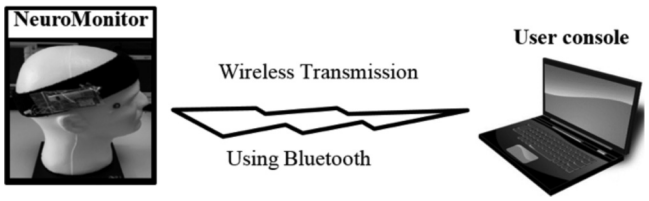

Fig. 7. The test-setup depicted with the NeuroMonitor (NM) EEG device communicating to a remote computer.

3.1. Test-Setup Components

For the algorithm development and implementation, primarily two software tools were utilized: (a) PSoC Creator 3.0 (for MCU programming) and (b) MATLAB (Remote user console). Before implementing the algorithm on PSoC-3 MCU, it was first verified off-chip using Microsoft Visual Studio C++ 2010, without the implementation of the ring buffer. Figure 7 depicts the test setup, which mainly includes the ambulatory NM EEG device and the MATLAB tool-based User console to receive the raw and clean EEG packets sent by the NM device via Bluetooth wireless transmission.

Our custom NM EEG device was utilized for capturing raw EEG signal and on-chip processing. The NM is a miniature, lightweight, two-channel referential montage-based EEG device that is deployable in real-life settings [Mahajan et al. 2014; Consul-Pacareu et al. 2014]. For this work, NM firmware was modified to implement the proposed algorithm on the PSoC-3 MCU on the NM board, and wirelessly transmit both raw and clean EEG signals to the remote console. The wireless transmission was performed using Bluetooth (Serial Port Profile, SPP) at a baud rate of 115.2KB/s. Both signals were transmitted so the algorithm could be verified; however in deployment, only processed data can be sent. The commercial, disposable, adhesive, pre-gelled Ag/AgCl electrodes (GS-26, Bio-Medical Instruments, Warren, MI) suitable for EEG data collection from the prefrontal cortex were used in the NM device with a sampling rate of 256 sps. The on-chip microcontroller PSoC-3 belongs to CY8C38 family having 8-bit 8051 CPU along with other peripherals of an 8KB RAM, 64KB Flash memory, three 62MHz internal oscillators, and on-chip 16-bit ADCs interfaced with an analog mux (AMUX).

3.2. Data Acquisition

The commercial disposable adhesive pre-gelled GS-26 electrodes used in NM device contained a 0.5% saline base gel on a 10mm flat pellet Ag/AgCl electrode surrounded by a paper-thin transparent self-adhesive tape disc of 1 inch in diameter [Consul-Pacareu et al. 2014]. Electrodes were positioned at FP1 and FP2 scalp locations on a subject (based on 10–20 International electrode system) having mastoid as the reference.

For the proposed hybrid algorithm implementation on hardware in this work, three datasets of a single subject pertaining to only a single representative channel (FP1 electrode) were utilized; however, the algorithm is not specific to this electrode and is expected to function equally for any electrode location. The captured raw data was processed using the PSoC-3 MCU and transmitted wirelessly using Bluetooth to the remote user console for further analysis as discussed earlier.

3.3. Remote User Console

The remote user console serves as the remote data acquisition software and was written using the MATLAB software tool. It receives packets of 537 bytes long via Bluetooth serial port (SPP profile) containing a Header section (9 bytes), raw EEG data (176 bytes), and clean EEG data (352 bytes). As shown in Figure 4(b), a 9-bytes-long header was used to ensure the received packet integrity at the user console by checking the packet start key (1^{st} byte) and the sequential packet count (8^{th} and 9^{th} bytes) to detect a packet miss. In the case of any data loss (packet miss), the user gets notified by the missed packet count in the Graphical User Interface (GUI) panel of data acquisition software [Consul-Pacareu et al. 2014]. Upon receiving the data packet successfully, acquisition software separates raw and processed data from the received 537 bytes of the buffer.

The 16-bit long raw data was sent as 2 bytes per sample while the clean EEG data is a float that requires 4 bytes. The processed data was then reformed to represent a 16-bit data. Next, the reformed data was scaled to the original microvolt levels to allow proper comparison of clean data with the raw data. Finally, the raw and processed EEG data were stored as a CSV file for further analysis.

A performance evaluation of the results of the proposed hybrid algorithm was also carried out at the remote user console. The 6 bytes of the header for OA detection zone indication were used to visually validate the OA detection algorithm executed on PSoC-3 MCU in real-time. Also, qualitative and quantitative analyses were performed offline at the user console from data stored in CSV files containing received raw and clean EEG data.

4. RESULTS

4.1. Ring Buffer Implementation Verification

It was important to first verify the ring buffer performance, as it is a critical validation of the real-time hardware processing based on proposed algorithm. For this purpose, only the code with ring buffer performing overlapping for raw and clean EEG was tested in real-time by skipping off OA detection and removal algorithms for the instance. To authenticate the performance of the ring buffer in real-time, the raw and clean EEG data should contain exactly the same values at the receiver since OA removal processing is disabled for this verification. The implemented ring buffer and overlapping methods worked perfectly with no mismatches (Figure 8). The raw and clean EEG received at the user console were plotted for visual comparison at various data sections, and it was observed that both data streams matched perfectly without any discrepancy, thus verifying the overlapped ring-buffer implementation.

4.2. Raw vs. Clean EEG Data

After verifying the ring buffer consistency, the hybrid OA removal algorithm was then enabled along with the ring buffer to observe the performance of the implemented algorithm. While comparing raw and clean EEG data, it was noticed that the proposed hybrid OA removal algorithm successfully de-noised the existing eye blinks in the raw EEG data. The test was carried out for three datasets of EEG recordings from a single subject, and a representative result for Dataset-1 is shown in Figure 9. The detected

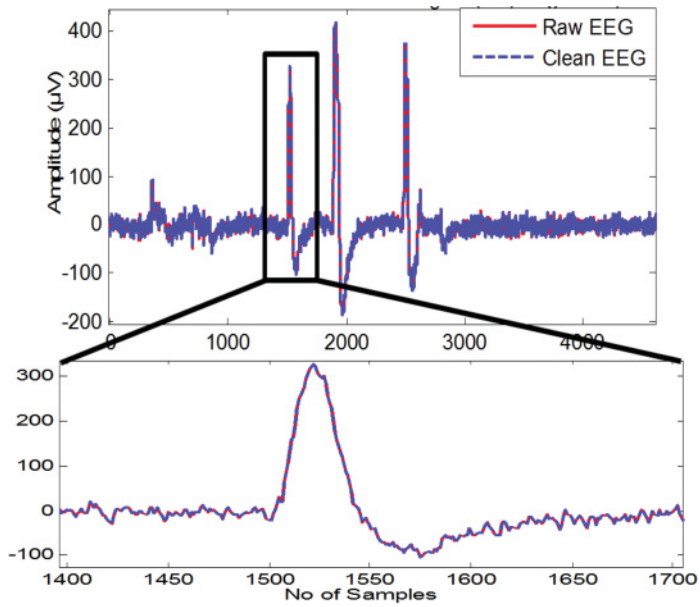

Fig. 8. Ring buffer real-time output verification on remote user console. (Note: The cleaning algorithm is disabled for this test.)

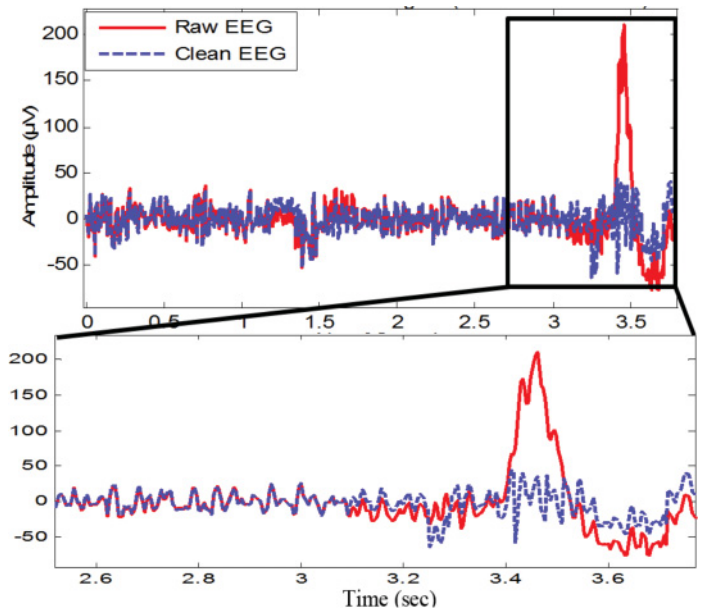

Fig. 9. PSOC-3 MCU processed hybrid algorithm result (FP1 electrode of Dataset-1).

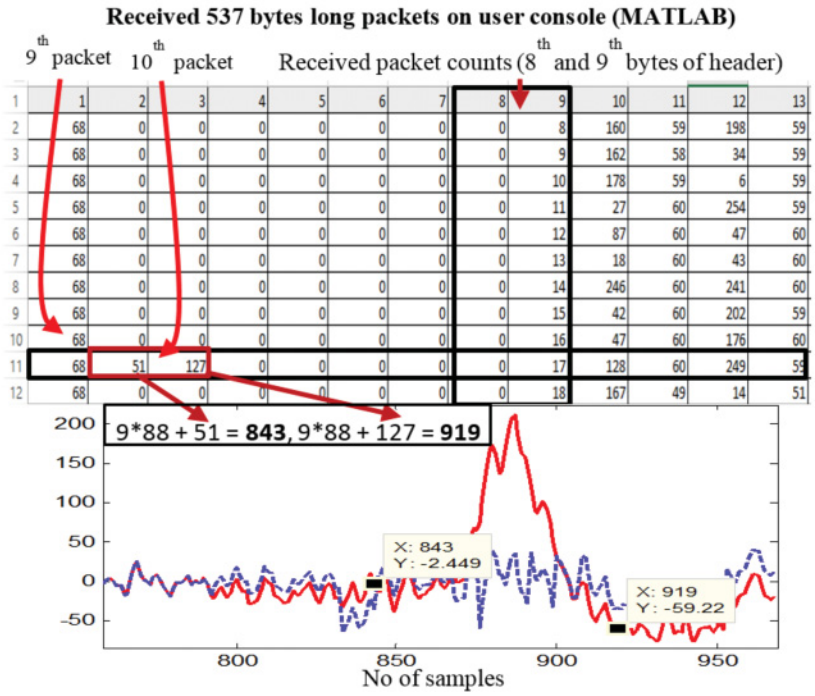

Fig. 10. Hybrid algorithm result verification (FP1: Dataset-1).

OA zones for Dataset-1 is shown in Figure 10, where the snapshots of MATLAB results of clean_EEG array header contents (index 1 to 9) are highlighted.

Every packet of length 537 bytes starts with the character D (received as corresponding ASCII value of 68), the next six bytes contain the OA zones (if detected), followed by the packet count numbers as highlighted in the Figure 10. As shown in this instance, prior to the OA zone, there were nine packets (88 samples in each) without OA detected. Thus, the calculation for OA zone starting and ending in the 10th packet, where OA was detected as depicted in Figure 10, can be performed and correlated with the raw EEG data plot (shown below the snapshot in Figure 10). The results demonstrate visual match with the actual position of the eye blink zone. This example demonstrates that the OA detection algorithm (AM) worked as per expectation when implemented on PSoC-3 hardware to operate in real time. Furthermore, the functional verification of de-noised OA zone can also be observed in Figure 9. This depicts that the OA removal algorithm implemented on PSoC-3 MCU performed satisfactorily as desired in compliance with the OA detection within the epoch.

For the small region of the raw and clean EEG data as depicted in the zoomed-inset plot for Dataset-1 of Figure 11, it can be observed that in non-OA zone, the signals show a little discrepancy and do not exactly overlap each other, which does not occur if the algorithm is implemented offline on the remote computer [Majmudar et al. 2015]. After investigating this discrepancy, it was determined that the reason for this mismatch is the difference in mean adjustments, which differs from the raw and the clean EEG data. For the clean EEG, the mean was calculated in real-time on PSoC-3 MCU as the algorithm runs on that hardware, whereas for the raw EEG, it was carried out later in MATLAB before the comparative study. Thus, resolution of the data and method differs for calculating mean in two cases, which led to this slight mismatch of EEG

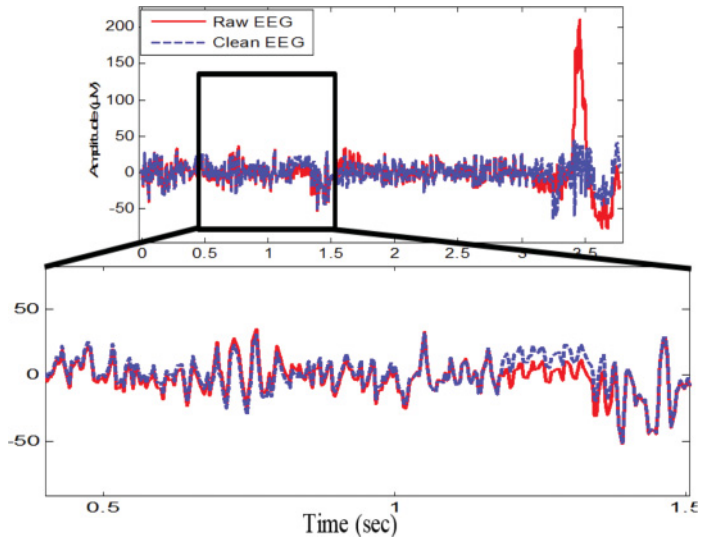

Fig. 11. Non-OA zone data mismatch: Raw vs. clean EEG (FP1 electrode of Dataset-1).

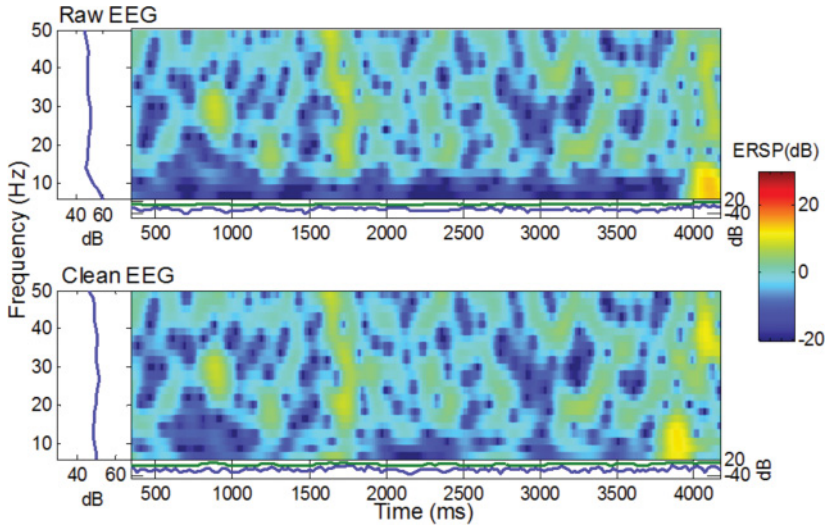

Fig. 12. Time-Frequency Analysis (TFA) plot for subject-1 EEG data (FP1).

data at non-OA zones. This mismatch does not create any significant adverse effects on the received EEG signal but this can also be resolved by adding a MATLAB script to extract and calculate the exact epochs considered in real-time on PSoC-3, then carry out the mean computation for the raw EEG data.

4.3. Performance Evaluation

Figure 12 illustrates a representative TFA plot for the raw and clean EEG data for subject 1 (FP1 electrode). The OA contains high-energy contents (higher dB) at low frequencies (below 10Hz) between 4s to 4.5s in the raw EEG data as depicted in Figure 12. After cleaning the data with the proposed hybrid algorithm in real-time,

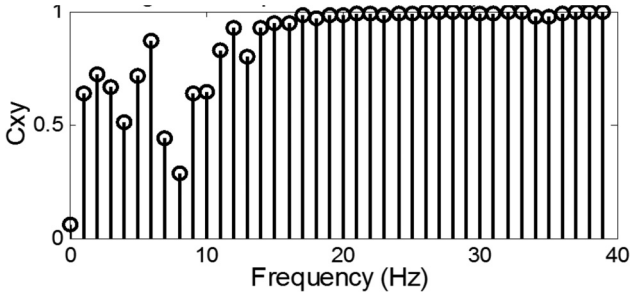

Fig. 13. MSC plot for raw vs clean EEG (FP1: Dataset-1).

Table III. Performance Metrics for CC

Dataset	Zone	Correlation of Coefficient	
		Blink 1	Blink 2
1	**OA zone**	0.2476	NA
	Non- OA	0.9981	
2	**OA zone**	0.1255	NA
	Non- OA	0.9459	
3	**OA zone**	0.6303	0.6096
	Non- OA	0.9839	

the corresponding location is free from high-energy content while the neuronal information is preserved (at higher frequencies at OA zone). Slight introduction of artifact is observed prior to OA zone (between 3.8s to 4s) where OA zone is detected, between 30Hz to 40Hz at OA zone, which is possibly the effect of Haar wavelet filter with DWT, computationally fast but prone to generating new artifacts, as we have previously demonstrated elsewhere [Khatun et al. 2015].

MSC analysis was carried out between raw and clean EEG separately for OA and non-OA zones. For OA zones, the clean EEG data at the lower frequency components, where OA resides, should show less coherence while higher than 16Hz frequency components should show maximum coherence ('1') with the raw EEG data. The result of MSC plot for the frequencies between 0Hz and 40Hz (Dataset-1) for OA zone is shown in Figure 13. Here, the low coherence values at lower frequency ranges of 0.5Hz to 16Hz indicates significant removal of artifacts whereas higher than 16Hz MSC is nearly coherent to '1'. This depicts minimal alteration of the neuronal signal components at those frequencies. For the non-OA zone, the MSC values were all '1' (plot not shown).

The CC was computed for OA zones and non-OA zones separately, and the results for the three datasets are tabulated in Table III. From the lesser values of CC in the OA zones, it is evident that the OA was effectively de-noised by suppressing the spikes. Furthermore, it was also observed that, similar to our previous results using MATLAB based OA removal with the proposed algorithm [Majmudar et al. 2015], CC values of the non-OA zones were not exactly '1'. The reason for this is, as mentioned before, that there is a small discrepancy in raw EEG data and cleaned EEG data because of the mean adjustment calculation difference. Nonetheless, the CC values for non-OA zones were close to '1' indicating a very good agreement between the raw and clean EEG data. These results show evidence that the proposed algorithm preserves the critical neural information in both OA and non-OA zones.

Table IV. Microcontroller-Unit Memory Usage Summary

PSoC-3 CY8C38 family	8-bit 8051 CPU
RAM	8KB
Flash memory	64KB
Used RAM	67.9% (5.56KB)
Used Flash memory	28.1% (18.1KB)

4.4. MCU Memory Performance

Finally, Table IV lists the total flash memory and RAM utilized by the MCU when the proposed OA removal algorithm is implemented, demonstrating the computational requirement of our proposed hybrid algorithm, which is hardware efficient. From Table IV, it is clear that the entire code implemented on PSoC-3 still leaves more than 30% of RAM and more than 70% of flash memory, which can be utilized for any additional algorithms/functionalities such as real-time feature extraction or classification to be implemented along with the proposed hybrid OA removal algorithm. Additionally, a higher power MCU can be used to implement a complete system with real-time EEG data capturing and its analysis entirely on the micro-controller hardware. Also, the execution time of the proposed hybrid OA removal algorithm on the MCU hardware was very small, and the clean EEG epochs after processing, packaging, and wireless transmission were received remotely within a latency period of 3 seconds.

5. DISCUSSION AND CONCLUSIONS

In this article, a proposed hybrid algorithm to remove OA from single-channel real-time EEG data implemented on the microcontroller hardware-based wearable EEG device (NeuroMonitor) is demonstrated. The hybrid algorithm comprised of an algebraic method (AM)-based OA detection, followed by DWT-based decomposition for OA removal of only the detected OA zones. The MCU fully autonomously executed the hybrid algorithm on a single-channel EEG data in real-time using 0.5s of EEG epochs. The algorithm was implemented with 0.5s EEG epochs with the overlapping window technique to ensure accurate OA detection without missing any OA event, even if it occurs at the epoch edges. The ring buffer implementation on MCU used for this overlapping technique showed proper execution and was functionally verified. Moreover, the proposed OA removal method was independently functionally verified for OA zone detection using algebraic method (AM), and for OA cleaning using the DWT method with the Haar wavelet basis function. This combination is computationally fast but prone to introduce small artifacts at higher frequencies. This limitation can be improved in future work by implementing the algorithm using other smooth basis functions (e.g., sym3 or coif3) in combination with the SWT algorithm using UT that is less prone to introduce artifacts [Khatun et al. 2015].

The TFA plot indicated that the algorithm could remove high-energy contents of OA while preserving neuronal-information-related energy contents outside OA zones, as well as for higher frequencies within OA zones. The MSC plot demonstrated that the raw EEG data was only altered for the lower frequency range where the OA resides while preserving the non-blink frequency ranges ($>$16Hz), which have potential to be neuronal information. Similarly, CC values showed that there was significant suppression of the signals in OA zones while insignificant differences in non-OA zones, which denotes that the neuronal information in non-OA zone remains unchanged.

This proposed hybrid OA removal algorithm implemented on PSoC-3 MCU (CY8C38), utilized less than 70% of RAM and less than 30% of the flash memory which implies that the algorithm has all the prospects to get extended for any further analysis such as feature extraction or classification to be implemented along with the proposed OA removal algorithm in real-time on the MCU. While the throughput of the

system maintained the constraint of input data sampling rate, the clean EEG data was received on the user console within nearly 3s of latency period indicating soft real-time execution. The reduction in latency of the algorithm's execution can be achieved by further reducing the FIR filter order on MCU hardware to reduce the computational complexity. In addition, the algorithm could be implemented on a more powerful MCU instead of PSoC-3 microcontroller, which would make the latency smaller. This fully autonomous algorithm can run on practically any deployable EEG device for its real-time analysis and feedback in a closed loop. Moreover, this hybrid approach can also be applied for any number of multichannel EEG systems, because the algorithm is independent of EEG data from other channels. Thus, it is widely applicable and versatile in nature. Finally, the proposed OA removal technique discussed here has significant promise in wearable technologies for real-time applications, and can be considered as a stepping stone for microcontroller implementable, real-time, single-channel OA removal technique for EEG systems for neuromodulation and neurofeedback. This new technique might be applied for diagnosis and therapy monitoring of patients with neurological disorders as well as monitoring the health and well-being of healthy individuals for improved performance evaluation, cognitive load assessment, and depression management. The challenges span from technological domain includes real-time feedback, power supply, and usability issues, as well as psychological aspects such as human behavior, data security issues, and privacy concerns.

ACKNOWLEDGMENTS

The authors would like to thank Ruhi Mahajan, Graduate student, Electrical and Computer Engineering, University of Memphis, for providing help in algorithm development and implementation aspects.

REFERENCES

Raymundo Cassani, Tiago H. Falk, Francisco J. Fraga, Paulo A. M. Kanda, and Renato Anghinah. 2014. The effects of automated artifact removal algorithms on electroencephalography-based Alzheimer's disease diagnosis. *Front Aging Neurosci.* 6, Article 55, (March 2014), 13.

Yu M. Chi, Patrick Ng, and Gert Cauwenberghs. 2013. Wireless noncontact ECG and EEG biopotential sensors. *ACM Trans. Embedd. Comput. Syst.* 12, 4, Article 103 (June 2013), 19.

Sergi Consul-Pacareu, R. Mahajan, N. Sahadat, and B. I. Morshed. 2014. Wearable ambulatory 2-channel EEG NeuroMonitor platform for real-life engagement monitoring based on brain activities at the prefrontal cortex. In *Proceedings of the 2014 IAJC-ISAM International Conference*, Paper 78, 12.

A. Delorme and S. Makeig. 2004. EEGLAB: An open source toolbox for analysis of single-trial EEG dynamics. *J Neurosci. Meth.* 134 (2004), 9–21.

H. T. Gorji, A. Koohpayezadeh, and J. Haddadnia. 2013. Ocular artifact detection and removing from EEG by wavelet families: A comparative study. *J. Inf. Engin. Appl.* 3 (2013), 39–47.

C. A. Joyce, I. F. Gorodnitsky, and M. Kutas. 2004. Automatic removal of eye movement and blink artifacts from EEG data using blind component separation. *Psychophysiology* 41 (2004), 313–325.

Saleha Khatun, Ruhi Mahajan, and Bashir I. Morshed. 2015. Comparative analysis of wavelet-based approaches for reliable removal of ocular artifacts from single channel EEG. In *Proceedings of the IEEE Electro/Information Technology (EIT)*, 335–340.

V. Krishnaveni, S. Jayaraman, L. Anitha, and K. Ramadoss. 2006. Removal of ocular artifacts from EEG using adaptive thresholding of wavelet coefficients. *J. Neur. Engin.* 3 (2006), 338.

P. S. Kumar, R. Arumuganathan, K. Sivakumar, and C. Vimal. 2008. A wavelet-based statistical method for de-noising of ocular artifacts in EEG signals. *Int. J. Comput. Sci. Netw. Secur.* 8 (2008), 87–92.

R. Lloyd, R. Goulding, P. Filan, and G. Boylan. 2015. Overcoming the practical challenges of electroencephalography for very preterm infants in the neonatal intensive care unit. *Acta Paed.* 104 (2015), 152–157.

Ruhi Mahajan, C. A. Majmudar, S. Khatun, B. I. Morshed, and G. M. Bidelman. 2014. NeuroMonitor ambulatory EEG device: Comparative analysis and its application for cognitive load assessment. In *Proceedings of IEEE Healthcare Innovations and Point-of-Care Technologies Conference*, 133–136.

Ruhi Mahajan and B. I. Morshed. 2015. Unsupervised eye blink artifact denoising in EEG data with modified multiscale sample entropy, kurtosis and wavelet-ICA. *IEEE J. Biomed. Health Inform.* 19, 1 (Jan. 2015), 158–165.

Charvi A. Majmudar, Ruhi Mahajan, and Bashir I. Morshed. 2015. Real-time hybrid ocular artifact detection and removal for single channel EEG. In *Proceedings of IEEE Intl Conf Electro/Information Technology (EIT)*, 330–334.

Fabien Masse, Martien van Vussel, Aline Serteyn, Johan Arends, and Julien Penders. 2013. Miniaturized wireless ECG monitor for real-time detection of epileptic seizures. *ACM Trans. Embedd. Comput. Syst.* 12, 4, Article 102 (June 2013), 21.

M. Mboup. 2012. Neuronal spike detection and localisation via Volterra filtering. In *Proceedings of the IEEE International. Workshop on Machine Learning for Signal Processing.* 1–5.

B. I. Morshed and A. Khan. 2014. A brief review of technologies and challenges to monitor brain activities. *J. Bioengin. Biomed. Sci.* 4, 1 (2014), 1–10.

Yunyong Nam, Seungmin Rho, and Chulung Lee. 2013. Physical activity recognition using multiple sensors embedded in a wearable device. *ACM Trans. Embedded. Comput. Syst.* 12, 2, Article 26 (Feb. 2013), 14.

Borna Noureddin. 2010. *Online Removal of Eye Movement and Blink Artifacts from EEG Signals without EOG*. Ph.D. Dissertation. The University of British Columbia, Vancouver, B.C., Canada.

Hong Peng, Dennis Majoe, and Thomas Kaegi-Trachsel. 2011. Design and application of a novel wearable EEG system for e-healthcare. In *Proceedings of the International Workshop on Ubiquitous Affective Awareness and Intelligent Interaction*. ACM, New York, NY, 1–8.

S. V. Ramanan, N. Kalpakam, and J. Sahambi. 2004. A novel wavelet-based technique for detection and de-noising of ocular artifact in normal and epileptic electroencephalogram. In *Proceedings of the Brain Inspired Cognitive Systems Conference.* 2, 1027–1031.

M. H. Soomro, N. Badruddin, M. Z. Yusoff, and M. A. Jatoi. 2013. Automatic eye-blink artifact removal method based on EMD-CCA. In *Proceedings of the ICME International Conference on Complex Medical Engineering (CME).* 186–190.

K. T. Sweeney, S. F. McLoone, and T. E. Ward. 2013. The use of ensemble empirical mode decomposition with canonical correlation analysis as a novel artifact removal technique. *IEEE Trans. Biomed. Engin.* 60, (2013), 97–105.

M. Teplan. 2002. Fundamentals of EEG measurement. *Measurement Sci. Rev.*, 2, (2002), 1–11.

Z. Tiganj, M. Mboup, C. Pouzat, and L. Belkoura. 2010. An algebraic method for eye blink artifacts detection in single channel EEG recordings. In *Proceedings of the 17th International Conference on Biomagnetism Advances in Biomagnetism–Biomag*. 175–178.

Received December 2015; revised March 2016; accepted May 2016